ARTICLE IN PRESS

Available online at www.sciencedirect.com

SCIENCE DIRECT®

Control Engineering Practice ▮ (▮▮▮▮) ▮▮▮–▮▮▮

CONTROL ENGINEERING PRACTICE

www.elsevier.com/locate/conengprac

Kinematic and dynamic identification of parallel mechanisms ☆

Pierre Renaud[a,1], Andres Vivas[a], Nicolas Andreff[b,c,*], Philippe Poignet[a], Philippe Martinet[c], François Pierrot[a], Olivier Company[a]

[a] *LIRMM, CNRS-Univ. Montpellier II, 34090 Montpellier, France*
[b] *LaRAMA, Univ. Blaise Pascal - IFMA, 63175 Aubière, France*
[c] *LASMEA, CNRS - Univ. Blaise Pascal, 63177 Aubière, France*

Received 10 September 2004; accepted 27 June 2005

Abstract

In this paper, we provide a comprehensive method to perform the physical model identification of parallel mechanisms. This includes both the kinematic identification using vision and the identification of the dynamic parameters. A careful attention is given to the issues of identifiability and excitation. Experimental results obtained on a H4 parallel robot show that kinematic identification yields an improvement in the static positioning accuracy from some 1 cm down to 1 mm, and that dynamic parameters are globally estimated with less than 10% relative error yielding a similar error on the control torque estimation.

Keywords: Physical model identification; Kinematic identification; Kinematic calibration; Inertial and friction parameters; Parallel mechanisms; Computer vision

1. Introduction

Parallel mechanisms are emerging in the industry (machine-tools, high-speed pick-and-place robots, flight simulators, medical robots, for instance). Indeed, these mechanisms have for main property their end-effector connected with several kinematic chains to their base, rather than one for the standard serial mechanisms. This allows parallel mechanisms to bear higher loads, at higher speed and often with a higher repeatability (Merlet, 2000). However, their large number of links and passive joints often limit their performance in terms of accuracy (Wang & Masory, 1993). Therefore, the kinematic parameters of such mechanisms have to be identified by the so-called kinematic identification (or kinematic calibration).

Moreover, in order to achieve high speed and acceleration for pick-and-place applications or precise motion in machining tasks, an accurate dynamic modeling is usually required. This will also increase the quality of their simulation in order to improve their design and/or to compute advanced model-based robust controllers such as moving horizon control schemes. After completing the kinematic calibration, the second difficulty is then to estimate the physical parameters including mass, inertia and frictions of the dynamic model.

1.1. State of the art

1.1.1. Kinematic identification

There exist several classes of methods to perform kinematic identification of parallel mechanisms (Fig. 1).

☆This work was supported by the MAX project of the CNRS ROBEA program and by Région d'Auvergne.

*Corresponding author. LAMI-LASMEA, Institut Francais de Mecanique Avancee, Campus de Clermont-Ferrand, Les Cezeaux, 63175 Aubière, France. Tel.: +33 4 73 28 80 66; fax: +33 4 73 28 81 00.
E-mail addresses: renaud.pierre@mail.insa-strasbourg.fr (P. Renaud), vivas@lirmm.fr (A. Vivas), andreff@ifma.fr (N. Andreff), poignet@lirmm.fr (P. Poignet), martinet@lasmea.univ-bpclermont.fr (P. Martinet), pierrot@lirmm.fr (F. Pierrot), company@lirmm.fr (O. Company).

[1] P. Renaud was jointly with LaRAMA and LASMEA when doing his Ph.D. on this work.

0967-0661/$ - see front matter © 2005 Elsevier Ltd. All rights reserved.
doi:10.1016/j.conengprac.2005.06.011

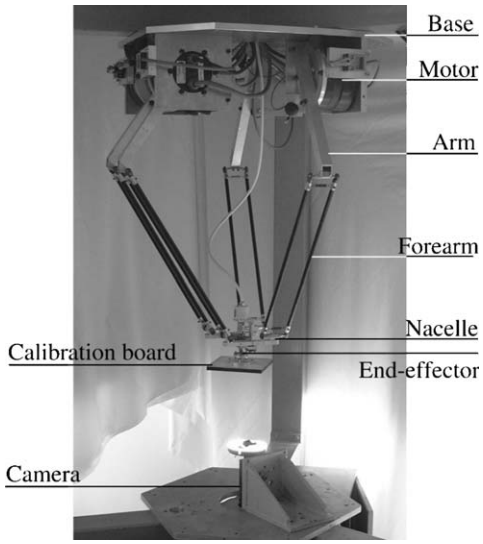

Fig. 1. A typical set-up for vision-based identification of a parallel mechanism: the H4 mechanism (Pierrot et al., 2001) and the vision-based measuring device.

The first one relies on the application of mechanical constraints on the end-effector or the mechanism legs (Daney, 1999; Khalil & Besnard, 1999). This class of methods only needs joint measurements, but is hard to use in practice since applying mechanical constraints requires an accurate extra mechanism. Moreover, such methods reduce the workspace size and therefore the identification efficiency (Besnard & Khalil, 2001). A second class of methods (Khalil & Murareci, 1997; Wampler & Arai, 1992; Zhuang, 1997), known as self-calibration, relies on the notion of redundant metrology: adding extra proprioceptive sensors at the usually uninstrumented joints of the mechanism allows for identification in the whole available workspace and only requires joint measurements. However, it is hard in practice to add these extra sensors on an existing mechanism and sometimes almost impossible (think of a spherical joint).

The third class of methods is based on the forward kinematic model and comes directly from the methods developed for serial mechanisms. Such methods minimize a non-linear error between a measure of the end-effector pose and its estimation from the measured joint values through the forward kinematic model (Masory et al., 1993; Visher, 1996). However, in general, parallel mechanisms only have a numerical evaluation of the latter, which may lead to numerical unstabilities of the identification (Daney, 1999).

On the opposite, for parallel mechanisms, the inverse kinematic model can usually be easily derived (Merlet, 2000). Therefore, the most natural method to perform identification of a parallel mechanism is to minimize an error between the measured joint variables and their corresponding values, estimated from the measured end-effector pose through the inverse kinematic model (Zhuang et al., 1995; Zhuang et al., 1998). This method seems indeed to be the most numerically efficient among the identification algorithms for parallel structures (Besnard & Khalil, 2001). Nevertheless, it is constrained by the need for accurate measurement of the full end-effector pose (i.e. both its position and its orientation). Some adapted measuring devices have been proposed (e.g. laser tracking systems (Koseki et al., 1998; Vincze et al., 1994) or mechanical devices, Geng & Haynes, 1994; Jeong et al., 1999) that are either expensive or limitative as workspace is concerned. Vision could constitute an adequate sensor (Zhuang & Roth, 1996; Zou & Notash, 2001), that we hence propose to use in this article.

1.1.2. Dynamic parameters identification

The experimental identification of serial mechanisms dynamic parameters has been extensively investigated within a statistical framework (Gautier & Poignet, 2001; Olsen & Petersen, 2001). Assuming random measurement errors with known statistical characteristics, the maximum likelihood (ML) estimator makes possible to derive reliable parameter estimates with confidence intervals. Usually the inverse model expressing the motor torque input as a function of the state variables is used to estimate the parameter vector through a weighted least squares (WLS) solution (Gautier & Poignet, 2001) since this model can be linearly written with respect to the parameters to be estimated.

Similarly, the dynamic model of parallel mechanisms can also be expressed in a linear relation with respect to the dynamic parameters. Therefore, in this paper, we focus on the estimation of the dynamic parameters of the rigid multibody closed loop structure: the parameters are estimated by a classical WLS technique. The main difficulty of approach lies in the estimation of the end-effector dynamics.

1.2. Contribution and outline

The main contribution of this paper is to provide the reader with a comprehensive method for identifying the complete physical model of a parallel robot. Hence, we identify the kinematic parameters, describing the geometry of the robot, and the dynamic physical parameters, describing the effects of masses, inertias and friction on the dynamical behavior of the robot.

Two algorithms are given for the vision-based kinematic identification, depending on which of the implicit or the inverse kinematic models is available for a given parallel robot. Using vision allows for unexpensive and accurate measurement of the end-effector position and orientation. A method is also provided for the identification of the dynamic physical

parameters. In both cases, the algorithms can be extended to every parallel robot and we pay a great attention to the issues of identifiability and excitation. These contributions are validated through extensive experimental results, obtained with the H4 robot.

The remainder of this paper is the following. Section 2 is devoted to the modeling of the H4 robot. Then, Section 3 presents the kinematic identification algorithms while Section 4 presents the dynamic identification method. Finally, before concluding, Section 5 displays the experimental results.

2. Modeling

The H4 robot has 4 degrees of mobility (3 translations plus 1 rotation around the vertical axis) provided that the four-bar mechanisms in the arms are articulated parallelograms. We assume in the following that this is true.

2.1. Kinematic models

One can define several models of the H4, whether one stays at CAD level or introduces additional parameters to take into account possible violations of the associated hypotheses.

The CAD model of the H4 robot (Pierrot et al., 2001), gives the following so-called implicit model (Wampler et al., 1995) expressing the closure of the kinematic chain around each leg, under the hypothesis of the existence of some symmetries in the mechanism (Fig. 2)

$$L^2 - l^2 - \|\overrightarrow{P_jA_j}\|^2 = -2\begin{pmatrix} \overrightarrow{P_jA_j}_x . l\cos(\alpha_j)\cos(q_j - q_{j_0}) \\ \cdots + \overrightarrow{P_jA_j}_y . l\sin(\alpha_j)\cos(q_j - q_{j_0}) \\ \cdots - \overrightarrow{P_jA_j}_z . l\sin(q_j - q_{j_0}) \end{pmatrix} \quad (1)$$

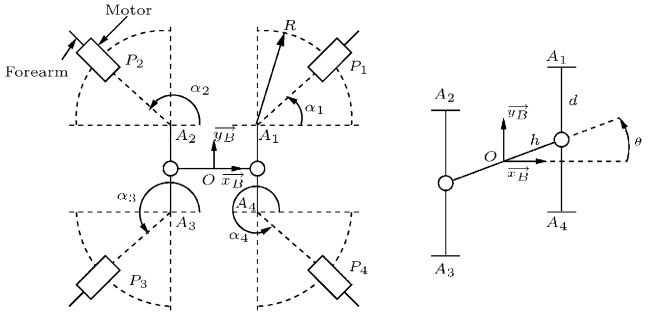

Fig. 2. CAD model of the H4 robot (viewed from the top): joint placement (left) and nacelle (right).

with L the arm length, l the forearm length (both the same for each leg), $\mathbf{q}$ the joint value vector, q_{j_0} the encoder offsets, P_j the motor position on the base, A_j are the attachment points of the parallelograms on the nacelle and other notation given in Fig. 2. Notice that the A_j's depend on the end-effector pose, denoted by $\mathbf{x} = [X, Y, Z, \theta]^{\mathrm{T}}$ and that the nacelle dimension d does not appear in this model. This implicit kinematic model is parameterized by 12 scalars: $(R, l, L, h, \alpha_j, q_{j_0}), j \in [1, 4]$ and will be referred to as the *implicit*-12 *model* in the sequel.

From this model, one can derive rather easily its inverse kinematic model (the so-called *inverse*-12 *model*):

$$q_j = q_{j_0} + 2A\tan\left(\frac{N + \varepsilon_j\sqrt{N^2 + M^2 - G^2}}{G + M}\right), \quad j \in [1, 4] \quad (2)$$

with $M = -2l(\overrightarrow{P_jA_j}_x\cos\alpha_j + \overrightarrow{P_jA_j}_y\sin\alpha_j)$, $N = 2l\overrightarrow{P_jA_j}_z$, $G = L^2 - l^2 - \|\overrightarrow{P_jA_j}\|^2$ and $\varepsilon_j = \pm 1$ depending on the assembly.

A more general implicit kinematic model can be used. Its base frame is attached to first joint center P_1, and its axis $\vec{z}_b$ parallel to the end-effector rotation axis. The other joints can be placed at any point $P_{j'} = (x_{j'}, y_{j'}, z_{j'}), j' \in [2, 4]$. Each joint may have any orientation (β_j, ψ_j), $j \in [1, 4]$ and the legs have independent arm and forearm lengths (L_j, l_j), $j \in [1, 4]$. Thus, this *implicit*-31 *model* involves a total of 31 parameters $(x_{j'}, y_{j'}, z_{j'}, \beta_j, \psi_j, q_{j_0}, l_j, L_j, h, d)$, $j' \in [2, 4]$, $j \in [1, 4]$ and becomes rather complicated:

$$\|L_j\overrightarrow{V_j} + \overrightarrow{W_j}\|^2 = l_j^2 \quad (3)$$

with

$$\overrightarrow{V_j} = \begin{bmatrix} \sin(q_j + q_{j_0})\cos(\beta_j)\sin(\psi_j) - \cos(q_j + q_{j_0})\cos(\psi_j) \\ -\sin(q_j + q_{j_0})\cos(\beta_j)\cos(\psi_j) - \cos(q_j + q_{j_0})\sin(\psi_j) \\ -\sin(q_j + q_{j_0})\sin(\beta_j) \end{bmatrix}$$

and

$$\overrightarrow{W_j} = \begin{bmatrix} X - x_j + (1 + \varepsilon_{1j} - \varepsilon_{1j}\cos(\theta))h \\ Y - y_j + d - \varepsilon_{1j}h\sin(\theta) \\ Z - z_j \end{bmatrix}.$$

In this case, it becomes cumbersome to find an inverse kinematic model, hence, we will restrict ourselves in the sequel to the use of the above three models.

2.2. Dynamic model

In first approximation, the dynamic model is computed by considering physical dynamics. Assuming that the drive torques are mainly used to move the motor inertia, the forearms, the arms and the nacelle, it is

written as follows:

$$\mathbf{\Gamma}_{mot} = \mathbf{I}_{mot}\ddot{\mathbf{q}} + \mathbf{J}^{\mathrm{T}}_{(\mathbf{x},\mathbf{q})}\mathbf{M}(\ddot{\mathbf{x}} - \mathbf{g}) + \mathbf{F}_v\dot{\mathbf{q}} + \mathbf{F}_c\,\mathrm{sign}(\dot{\mathbf{q}}), \tag{4}$$

where $\mathbf{I}_{mot}$ represents the motor inertia matrix (thanks to the design, the forearm inertia can be included as a part of the motor inertia and the inertial effects of the arms, manufactured in carbon materials, are neglected, Company & Pierrot, 1999; Pierrot et al., 2001), $\mathbf{M}$ contains the mass of the nacelle and its inertia, $\mathbf{J}_{(\mathbf{x},\mathbf{q})}$ is the Jacobian matrix of the inverse kinematic model, $\mathbf{g}$ is the gravity vector, $\mathbf{F}_v$ are the viscous friction coefficients and $\mathbf{F}_c$ are the Coulomb friction and the ‘˙’ notation represents the time derivation.

The matrix $\mathbf{I}_{mot}$ and $\mathbf{M}$ are given by

$$\mathbf{I}_{mot} = \Delta\left(\begin{bmatrix} I_{mot1} & I_{mot2} & I_{mot3} & I_{mot4}\end{bmatrix}^{\mathrm{T}}\right), \tag{5}$$

where $\Delta()$ is the diagonal matrix formed by its argument and

$$\mathbf{M} = \begin{bmatrix} M_{nac}\mathbf{I}_3 & \mathbf{0}_{3\times 1} \\ \mathbf{0}_{1\times 3} & I_{nac}\end{bmatrix}. \tag{6}$$

It is assumed that the joint positions $\mathbf{q}$, the nacelle acceleration $\ddot{\mathbf{x}}$ along the x, y and z directions and its orientation θ are measured.

Introducing $\mathbf{J}^{\mathrm{T}}_{(\mathbf{x},\mathbf{q})} = \begin{bmatrix}\mathbf{J}_{43}\ \mathbf{j}_4\end{bmatrix}$, where $\mathbf{J}_{43}$ is a matrix containing the first three columns of $\mathbf{J}^{\mathrm{T}}_{(\mathbf{x},\mathbf{q})}$ and $\mathbf{j}_4$ is its last column, the dynamic equation can be rewritten in a relation linear with respect to the dynamic parameters:

$$\mathbf{\Gamma}_{mot} = \begin{bmatrix} \Delta(\ddot{\mathbf{q}}) & \mathbf{J}_{43}\begin{bmatrix}\ddot{\mathbf{x}}\\ \ddot{\mathbf{y}}\\ \ddot{\mathbf{z}} - g\end{bmatrix} & \mathbf{j}_4\ddot{\theta} & \Delta(\dot{\mathbf{q}}) & \Delta(\mathrm{sign}(\dot{\mathbf{q}}))\end{bmatrix}\xi_d, \tag{7}$$

where ξ_d is the vector of the dynamic parameters to be estimated:

$$\xi_d = [I_{mot1}\ I_{mot2}\ I_{mot3}\ I_{mot4}\ M_{nac}\ I_{nac}\ \ldots \\ \ldots\ f_{v1}\ f_{v2}\ f_{v3}\ f_{v4}\ f_{c1}\ f_{c2}\ f_{c3}\ f_{c4}]^{\mathrm{T}}. \tag{8}$$

3. Kinematic identification

In this section, we give two alternate methods for calibrating a parallel mechanism using an exteroceptive measuring device (with immediate application to the case of vision). One is the classical method based on the inverse kinematic model and the other is based on the implicit kinematic model. In both cases, we show that one must introduce additional parameters owing to the use of an exteroceptive measurement of the end-effector pose.

3.1. Identification using the inverse kinematic model

The inverse kinematic model computes the joint variables $\mathbf{q}_c$ as a function of the end-effector pose ${}^b\mathbf{T}_e = ({}^b\mathbf{R}_e, {}^b\mathbf{t}_e)$ with respect to the base frame and the kinematic parameter vector ξ_k. Zhuang et al. (1998) proposed to form, for any pose ${}^b\mathbf{T}_{e_i}$, the following error

$$\varepsilon_i = \hat{\mathbf{q}}_i - \mathbf{q}_c({}^b\hat{\mathbf{T}}_{e_i}, \xi_k) \tag{9}$$

between the corresponding measured joint values $\hat{\mathbf{q}}_i$ and the computed ones $\mathbf{q}_c({}^b\hat{\mathbf{T}}_{e_i}, \xi_k)$, then to determine the kinematic parameters by measuring, with an exteroceptive sensor, m different poses ${}^b\hat{\mathbf{T}}_{e_i}, i \in [1, m]$, and finally estimate ξ_k by the non-linear minimization of the following cost function with respect to ξ_k:

$$\chi^2(\xi_k) = \varepsilon^{\mathrm{T}}\varepsilon, \quad \varepsilon = [\varepsilon_1^{\mathrm{T}}, \ldots, \varepsilon_m^{\mathrm{T}}]^{\mathrm{T}}. \tag{10}$$

However, this suggests that the end-effector pose can be measured in the base frame. Due to the use of an exteroceptive measuring device, this, in fact, cannot be achieved since one shall take into account the pose of the measuring device with respect to the base frame ${}^b\mathbf{T}_c$ and, which is not evident, the pose of the target of the measuring device with respect to the end-effector ${}^e\mathbf{T}_t$. Indeed, any measuring device needs a target, which can be a reflective cube for a laser tracker system, reflective amers for a theodolite or a physical interface part for a mechanical measuring machine. When using vision, the measuring device is composed of a fixed CCD camera and a target attached to the end-effector and gives the pose of the target with respect to the camera as shown by Lavest et al. (1998).

Formally, this implies that one measures poses of the target with respect to the measuring device ${}^c\mathbf{T}_{t_i}$, which are related to the end-effector poses with respect to the base by the unknown above-mentioned constant rigid transformations ${}^b\mathbf{T}_c$ and ${}^e\mathbf{T}_t = {}^t\mathbf{T}_e^{-1}$ through

$${}^b\mathbf{T}_{e_i} = {}^b\mathbf{T}_c\,{}^c\mathbf{T}_{t_i}\,{}^t\mathbf{T}_e \quad \forall i \in [1, m]. \tag{11}$$

Therefore, instead of the error in (9) one should use the following error:

$$\varepsilon_i = \hat{\mathbf{q}}_i - \mathbf{q}_c({}^b\mathbf{T}_c\,{}^c\hat{\mathbf{T}}_{t_i}\,{}^t\mathbf{T}_e, \xi_k). \tag{12}$$

Noting ξ_e the external parameters, i.e. the set of parameters describing ${}^b\mathbf{T}_c$ and ${}^t\mathbf{T}_e$, the problem of parallel mechanism kinematic identification based on the inverse kinematic model can be formally stated as the following non-linear minimization problem:

$$\min_{\xi_k, \xi_e} \sum_{i=1}^{m} \|\hat{\mathbf{q}}_i - \mathbf{q}_c({}^c\hat{\mathbf{T}}_{t_i}, \xi_k, \xi_e)\|^2. \tag{13}$$

3.2. Identification using the implicit kinematic model

Formally, the implicit kinematic model[2] is an equation relating the joint values, the end-effector pose and the kinematic parameters. In the case we are dealing with where the end-effector pose is measured, the implicit kinematic model takes the following generic expression:

$$\Psi(\mathbf{q}, {}^{c}\mathbf{T}_t, \xi_k, \xi_e) = 0. \tag{14}$$

Then, the problem of parallel mechanism kinematic identification based on the implicit kinematic model can be formally stated as the following non-linear minimization problem:

$$\min_{\xi_k, \xi_e} \sum_{i=1}^{m} \|\Psi(\hat{\mathbf{q}}_i, {}^{c}\hat{\mathbf{T}}_{t_i}, \xi_k, \xi_e)\|^2. \tag{15}$$

3.3. Identifiability

Calibrating a robot is an identification process and hence, one should take a careful look at the identifiability of the model parameters, i.e. one should be able to answer the following questions

- Can we estimate all the parameters in the model?
- If so, how to optimize the estimation?
- If not, why? and What is the subset of the parameters that can be estimated (identifiable parameters)?

The answers to those questions are related to the non-linear minimization problem numerical solution. Most of the time, people use iterative algorithms (such as Newton, Gauss or Levenberg–Marquardt algorithms) solving, at each iteration η, a linear least-square approximation of the cost function:

$$\frac{\partial \chi^2(\xi_\eta)}{\partial \xi}(\xi_{\eta+1} - \xi_\eta) = \chi^2(\xi_\eta), \tag{16}$$

where ξ_η is the ηth estimation of the parameters $\xi = \xi_k \cup \xi_e$ and $\chi^2(\xi)$ is, in our case, given by (13) or (15).

It is easy to understand that the estimation update step can only be done on the components of ξ that do not lie in the kernel of the regressor $\partial\chi^2(\xi_\eta)/\partial\xi$. A parameter which is in the kernel of the regressor at every iteration will hence not be identifiable, i.e. its value will not be updated from the a priori estimate. Therefore, much work was lead, in the case where all parameters are identifiable, on finding the so-called sufficient excitation (Daney, 2002; Gautier & Khalil, 1992; Swevers et al., 1997), that is, the experiment such that the regressor will have full rank and yield the best minimization of the estimation error. In the case of kinematic identification, this boils down to the selection of an optimal set of robot configurations (Nahvi & Hollerbach, 1996; Renaud et al., 2003).

However, there can be a so-called structural loss of rank (Besnard & Khalil, 2001; Khalil & Dombre, 2002). Indeed, the model can be such that whatever the excitation is, the regressor is always rank deficient. This means that there exist linearly dependent combinations between the columns of the regressor. Reminding that there is a one-to-one correspondence between the columns of the regressor and the parameters, one may define the set of base parameters which is the largest set of parameters (or combinations thereof) such that their associated columns are linearly independent.

Now, let us come back to kinematic identification with exteroceptive measurement of the end-effector pose and try to find the base parameters. Omitting the iteration subscript, the regressor is thus of the form

$$\frac{\partial \chi^2(\xi)}{\partial \xi} = \left[\frac{\partial \chi^2(\xi)}{\partial \xi_k} \quad \frac{\partial \chi^2(\xi)}{\partial \xi_e}\right]. \tag{17}$$

Loss of rank can occur in three cases:

3.3.1. Non-identifiable kinematic parameters

The kinematic parameters are identifiable if the model used for identification is minimally parameterized. This only depends on the mechanism itself and should have been checked already at modeling stage.

Formally, if there exist non-identifiable kinematic parameters, then there exists a full-rank matrix $\mathbf{A}_k$, a combination matrix $\mathbf{C}_k$ (possibly rank deficient) and a permutation matrix $\mathbf{P}_k$ (i.e. $\mathbf{P}_k^2 = \mathbf{I}$) such that

$$\frac{\partial \chi^2(\xi)}{\partial \xi_k} = \begin{bmatrix}\mathbf{A}_k & \mathbf{A}_k\mathbf{C}_k\end{bmatrix}\mathbf{P}_k. \tag{18}$$

Hence, we can reorder the parameter vector ξ_k with the permutation matrix $\mathbf{P}_k$ and then split the result into two parts: $(\mathbf{P}_k\xi_k)^T = (\xi_{k'}^{\mathrm{T}}, \xi_{k_{\overline{id}}}^{\mathrm{T}})$, where $\xi_{k'}$ corresponds to the full-rank matrix $\mathbf{A}_k$ and $\xi_{k_{\overline{id}}}$ corresponds to the dependent part $\mathbf{A}_k\mathbf{C}_k$. The vector $\xi_{k_{\overline{id}}}$ contains the non-identifiable kinematic parameters. They do not have any individual influence on the mechanism behavior and generate columns in the regressor that uselessly make the latter singular. Therefore, $\xi_{k_{\overline{id}}}$ can be thrown away (i.e. set to an arbitrary value, which can be zero or an a priori value) and the base parameters are to be found in $\xi_{k'}$.

3.3.2. Non-identifiable external parameters

External parameters only appear in (11). Therefore, non-identifiable external parameters are such that the end-effector pose with respect to the base is left

[2] We do not know of a parallel mechanism which does not have an analytical formulation of these closure equations. Note that usually the inverse kinematic model is extracted by algebraic manipulation from the implicit kinematic model.

unchanged if we modify them. Hence, they do not have any influence on the mechanism behavior. However, it is of importance to detect such non-identifiable external parameters to suppress the corresponding columns in the regressor that also uselessly make the latter singular. This can be done similarly as for the kinematic parameters by writing

$$\frac{\partial\chi^2(\xi)}{\partial\xi_e} = [\,\mathbf{A}_e \quad \mathbf{A}_e\mathbf{C}_e\,]\mathbf{P}_e \tag{19}$$

and splitting the external parameters in the non-identifiable external parameters $\xi_{e_{\overline{id}}}$ and the remainder $\xi_{e'}$.

Note that the loss of external parameters identifiability can be related to the number of degrees of *spatiality* of the mechanism (Renaud, 2003).

3.3.3. Coupled kinematic and external parameters

From the previous two cases, we can rewrite (17) as

$$\frac{\partial\chi^2(\xi)}{\partial\xi} = [\,\mathbf{A}_k \quad \mathbf{A}_e \quad \mathbf{A}_k\mathbf{C}_k \quad \mathbf{A}_e\mathbf{C}_e\,] \tag{20}$$

associated to the reordered set $[\xi_{k'}^{\mathrm{T}}, \xi_{e'}^{\mathrm{T}}, \xi_{k_{\overline{id}}}^{\mathrm{T}}, \xi_{e_{\overline{id}}}^{\mathrm{T}}]^{\mathrm{T}}$ of parameters.

Now, although $\mathbf{A}_k$ and $\mathbf{A}_e$ have full rank, their compound $(\mathbf{A}_k\ \mathbf{A}_e)$ may be rank deficient. Similarly as in the above two cases, we can split it into two parts: one full-rank matrix and one linearly dependent part. Thereby, we also reorder and then split the vector $(\xi_{k'}^{\mathrm{T}}, \xi_{e'}^{\mathrm{T}})^{\mathrm{T}}$ into two parts: the vector containing the base parameters ξ_{base} and a second part $\xi_{coupled}$ which contains the remaining parameters that cannot be identified.

Note that both parts contain kinematic *and* external parameters. Therefore, $\xi_{coupled}$ contains a part defining the mechanism behavior and a part related to the measure of the end-effector pose, while, together, these two parts do not appear in the error used for identification. This means that if one removes the exteroceptive measuring device at control time, then there will be missing kinematic knowledge in the model and therefore, the control will be inaccurate. A solution would be to turn oneself to identification methods without exteroceptive sensing or to keep the exteroceptive measure at control time (for instance, to use visual servoing techniques, Andreff et al., 2002).

4. Dynamic identification

4.1. Algorithm

The parameter vector ξ_d (8) is estimated as the solution of the WLS of an over-determined system obtained by sampling and filtering the dynamic model (7) along an exciting trajectory $(q, \dot{q}, \ddot{q})$ at successive sampled time $t_i, i = 1, \ldots, r$, r being the number of samples:

$$\mathbf{y} = \mathbf{W}\xi_d + \rho, \tag{21}$$

where $\mathbf{y}$ is the $(r \times 1)$ motor torque measurement vector, $\mathbf{W}$ is the $(r \times p)$ observation matrix obtained by sampling (7) along the exciting trajectory, p is the number of parameters to be estimated, ρ is the vector of errors.

It is usually assumed that ρ is a zero mean additive independent noise, with a standard deviation σ_ρ such that

$$\mathbf{C}_{\rho\rho} = E(\rho^{\mathrm{T}}\rho) = \sigma_\rho^2\mathbf{I}_r, \tag{22}$$

where E is the expectation operator, $\mathbf{I}_r$ the identity matrix.

To compute the WLS solution of (21), the r_j rows, corresponding to joint j equation, are weighted by the diagonal components of the error covariance matrix defined as follows:

$$\mathbf{C}_{\rho\rho} = (\mathbf{G}^{\mathrm{T}}\mathbf{G})^{-1}, \tag{23}$$

where $\mathbf{G}$ is a $(r \times r)$ diagonal matrix with the elements of $\mathbf{S}$ on its diagonal:

$$\mathbf{S} = \left[\mathbf{S}^1 \ldots \mathbf{S}^n\right], \quad \text{with} \quad \mathbf{S}^j = \left[\frac{1}{\hat{\sigma}_\rho^j} \cdots \frac{1}{\hat{\sigma}_\rho^j}\right], \tag{24}$$

where $\mathbf{S}^j$ is a $(1 \times r_j)$ row matrix and n is the number of joints (here, $n = 4$). An unbiased estimation $\hat{\sigma}_\rho^j$ is used from the regression on each joint j subsystem:

$$\hat{\sigma}_\rho^{j^2} = \frac{\|\mathbf{y}^j - \mathbf{W}^j\hat{\xi}_d^{\,j}\|^2}{(r^j - p^j)}, \tag{25}$$

where $\mathbf{y}^j, \mathbf{W}^j, \hat{\xi}_d^{\,j}, r^j, p^j$ are, respectively, the measurement vector, the observation matrix, a prior estimated parameters vector, the number of equations and the number of minimum parameters for each joint j subsystem.

The WLS vector solution $\hat{\xi}_{dw}$ minimizes the Euclidean norm of the vector of weighted errors ρ:

$$\hat{\xi}_{dw} = \min_{\xi_d}(\rho^{\mathrm{T}}\mathbf{G}^{\mathrm{T}}\mathbf{G}\rho), \tag{26}$$

where $\hat{\xi}_{dw}$ and the corresponding standard deviations $\sigma_{\hat{\xi}_{dw}}$ are calculated as the LS solution of (21) weighted by $\mathbf{G}$. The new system is given by

$$\mathbf{y}_w = \mathbf{W}_w\xi_d + \rho_w, \tag{27}$$

where $\mathbf{y}_w = \mathbf{G}\mathbf{y}$, $\mathbf{W}_w = \mathbf{G}\mathbf{W}$ and $\rho_w = \mathbf{G}\rho$.

4.2. Identifiability

The unicity of the solution depends on the rank of the observation matrix. The loss of rank can come from two origins:

- A structural rank deficiency which stands for any samples in $\mathbf{W}$. This problem of identifiability is

resolved by using the basic parameters which supply a minimal representation of the model (Gautier, 1991; Gautier & Khalil, 1990).
- A data rank deficiency due to a bad choice of noisy samples in $\mathbf{W}$. This is the problem of optimal measurement strategies which is solved using closed loop identification to track exciting trajectories (Gautier, 2000; Gautier & Khalil, 1992; Swevers et al., 1997).

Calculating the WLS solution of (21) from noisy discrete measurements or estimations of derivatives may lead to bias because $\mathbf{W}$ and $\mathbf{y}$ are non-independent random matrices. Then it is essential to filter data in $\mathbf{y}$ and $\mathbf{W}$, before computing the WLS solution. Data processing will be briefly detailed in Section 5.2.

5. Experiments

5.1. Kinematic identification

We now apply the comprehensive identification method to the H4 robot with the experimental set-up displayed in Fig. 1 and a 1024×768 pixel 7.5 Hz CCD camera.

5.1.1. Identifiability

Analyzing the models shows that in the three models, the transformations ${}^{t}\mathbf{T}_{e}$ and ${}^{b}\mathbf{T}_{c}$ contain non-identifiable external parameters. This is due to the fact that the end-effector only has one degree of freedom in rotation and can be related to results on hand-eye identification (Andreff et al., 2001). Moreover, in the implicit-31 model, the kinematic parameter d is coupled with the external parameter ${}^{b}y_{c}$, translation component of ${}^{b}\mathbf{T}_{c}$. Thus, only the a priori value of d can be used when needed. The consequence of this coupling between external and kinematic parameter is here a constant offset on the zero-reference point of the end-effector, which hopefully can be easily compensated for.

5.1.2. Data collection

We collected in a first step eight images of the identification target and used them for calibrating the measuring device. Then, we moved the robot in 27 uniformly distributed position in the workspace and in each position we rotated the nacelle in three different orientations (-50°, 0°, 50°), thus gathering 81 poses.[3] The computation of the condition number of the regressor (16) shows that this set is an adequate excitation. In each pose, we recorded an image and the corresponding joint values. Finally, 71 out of these 81 poses were randomly chosen for the kinematic identification.

[3]An automated image detection algorithm is used to simplify the experimental procedure.

Fig. 3. Validation by linearity check.

5.1.3. Validation

We validated the identification results with three validation procedures. First, using the 10 unused poses as independent validation data, we computed the mean and RMS error between the measured joint variables and their estimated value obtained with the identified inverse kinematic model. Second, in order to validate the results independently from the measuring device, we proceeded to linearity check (Fig. 3):

- The end-effector was manually moved along a straight ruler while recording the joint values in several stations.
- We applied a numerical estimation of the forward kinematic model to the joint values in each position with the estimated kinematic parameters. This gave us an estimation of each of the end-effector poses, from which we computed a least-square estimate of the straight line they are constrained to lie on.
- We computed the standard deviation with respect to the latter estimated straight line.

Third, to validate the inverse-12 model, we even went as far as control validation. Indeed, using the cartesian control mode of the robot, we required the end-effector to move to the four corners of a 100 mm square, twice with the CAD values of the parameters (to check the robot repeatability) and once with the estimated parameters.

5.1.4. Results

In Table 1, we give the a priori and identified values of the kinematic parameters. The residual validation tests are given in Table 2 and the linearity check along two approximatively orthogonal directions in Table 3. For

Table 1
A priori and identified kinematic parameters

Parameters		A priori values	Implicit-12 (CR) model	Inverse-12 (CR) model	Units
Lengths	h	60	61	61	mm
	L	480	488.6	487.2	mm
	l	260	259.8	259.6	mm
Joint positions	R	140	140.3	141.1	mm
	α_1	0	−0.05	−0.0015	rad
	α_2	3.1416	3.070	3.094	rad
	α_3	4.7124	4.678	4.675	rad
	α_4	4.7124	4.682	4.680	rad
Joint offsets	q_{1_0}	0	−0.0654	−0.0692	rad
	q_{2_0}	0	−0.0071	−0.0191	rad
	q_{3_0}	0	−0.0489	−0.0525	rad
	q_{4_0}	0	−0.0570	−0.0609	rad

Table 2
Residual test (in rad)

Joint variable	q_1	q_2	q_3	q_4
CAD model				
Mean error	$9.0e \times 10^{-2}$	$3.5e \times 10^{-3}$	$7.3e \times 10^{-2}$	$8.3e \times 10^{-2}$
RMS error	$9.0e \times 10^{-2}$	$3.7e \times 10^{-2}$	$7.4e \times 10^{-2}$	$8.3e \times 10^{-2}$
Implicit-12 *model*				
Mean error	$-8e \times 10^{-5}$	$-5e \times 10^{-5}$	$-1e \times 10^{-4}$	$-2e \times 10^{-5}$
RMS error	$1.1e \times 10^{-3}$	$1.2e \times 10^{-3}$	$1.1e \times 10^{-3}$	$1.1e \times 10^{-3}$
Inverse-12 *model*				
Mean error	$7.1e \times 10^{-5}$	$1.1e \times 10^{-4}$	$-7.7e \times 10^{-4}$	$-2.1e \times 10^{-4}$
RMS error	$1.4e \times 10^{-3}$	$1.3e \times 10^{-3}$	$1.4e \times 10^{-3}$	$2.6e \times 10^{-3}$

Table 3
Linearity check (in mm)

Direction	A priori	Implicit-12	Inverse-12	Implicit-31
1	1.3	0.5	0.49	0.59
2	2.3	0.49	0.58	1.1

the implicit-31 model, we only display the linearity check which shows that, as already stated in the literature (Schroer, 1993; Visher, 1996), the increase of the model complexity may reduce the identification accuracy.

The kinematic parameter variations are significant with length modification of several millimeters and variation of the angles defining the joint positions and joint offsets of the order of 2°. However, the use of inverse or implicit kinematic model does not, for that experiment, induce sharp modification of the identification efficiency. The linearity check is only slightly improved by the use of the implicit model (Table 3).

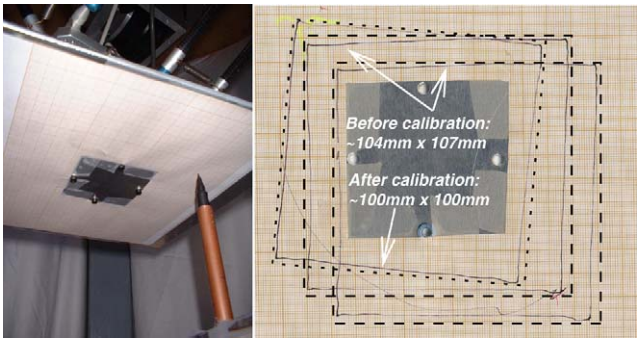

Fig. 4. Validation by control: set-up (left) and result (right).

One may note that the most important length variation is the forearm length L, with a modification of about 7 mm. This 7 mm modification seems rather huge compared to the a priori knowledge on this dimension. It has, however, been justified by better identification results when identifying the parameter rather than using its a priori value. It seems that the identification of this parameter enables us to compensate for the end-effector orientation modification, evaluated with the vision-based pose measurement in the order of 0.3°, that cannot be taken into account with this model.

Fig. 4 shows the results of the validation by control. One can see two trajectories (with super-imposed dashed approximating squares) obtained before identification for two different positions of the pen, which validate the repeatability of the robot. One can more interestingly see a third trajectory (with super-imposed dotted approximating square) obtained after identification. Note that the error reduces from about 1 cm down to 1 mm. Note also that using the a priori parameters rather than the identified ones yields an approximate positioning error of the nacelle of 26 mm and 0.022 rad.

5.2. Dynamic identification

5.2.1. Data collection and filtering

Joint velocities and accelerations are estimated, as well as the second-order derivative of the orientation θ, by a band-pass filtering of the position (or the orientation) obtained by the product of a low-pass filter in both the forward and the reverse direction (Butterworth) and from a derivative filter, obtained by a central difference algorithm without phase shift. The cut-off frequency ω_H of the low-pass filter should be chosen to avoid any distortion of magnitude on the filtered signals in the range [0 ω_{dyn}], where ω_{dyn} is the bandwidth of the position closed loop. A second filtering is implemented to eliminate the high-frequency noises in the motor torque. The vector $\mathbf{y}$ and each column of $\mathbf{W}$ are filtered (known as parallel filtering) by a low-pass filter and are resampled at a lower rate, keeping one sample over n_d

because there is no more signal in the range $[\omega_H, \omega_s/2]$ (ω_s is the sampling frequency). Because of the linearity of (21), the WLS is not sensitive to the distortion introduced by the parallel filtering. Here, we have $\omega_H = 130\,\text{Hz}$, $\omega_s = 1\,\text{kHz}$ and $\omega_{dyn} \leqslant 15\,\text{Hz}$.

Each component Γ_{mot_i} of the motor torques Γ_{mot} is estimated using a linear relation between torque and voltage applied to the amplifier:

$$\Gamma_{mot_i} = k_i V_i, \tag{28}$$

where V_i is the current reference (the control input) of the amplifier current loop and k_i the gain of the ith joint drive chain.

5.2.2. Results

Good identification results are obtained when good exciting trajectories are imposed to the robot. The quality of the exciting trajectories can be evaluated through a good condition number of the regressor $\mathbf{W}$ (Gautier & Poignet, 2001). Accordingly, we generate exciting trajectories containing slow motions (in such a case, friction will be preponderant) and high dynamic motions (inertia phenomena become preponderant). A concatenation of such trajectories is used.

In Table 4, the estimated parameters are presented with their confidence interval given as the relative standard deviation. The dynamic parameters are quite well estimated with relative standard deviation lower than 10%.

The validation of the identification results consists in comparing the measured torques with those obtained by computing the inverse dynamic model with the estimated parameters. As indicated above the measured torques are obtained from the current reference with (28). Figs. 5–8 exhibit cross validations with new trajectories that have not been previously used for the

Table 4
Estimated parameters using additional sensors

Parameters	Estimated values	Units	$\%\sigma_{\hat{X}_w}$
I_{mot1}	0.0167	N m^2	2.3695
I_{mot2}	0.0164	N m^2	2.3590
I_{mot3}	0.0176	N m^2	1.5776
I_{mot4}	0.0234	N m^2	1.1579
M_{nac}	0.984	Kg	0.4666
I_{nac}	0.0029	N m^2	3.7311
f_{v1}	0.2112	N m s/rad	4.7212
f_{v2}	0.1236	N m s/rad	7.5670
f_{v3}	0.1266	N m s/rad	5.2000
f_{v4}	0.1133	N m s/rad	5.6255
f_{c1}	1.2186	N m	2.0756
f_{c2}	1.0252	N m	2.3623
f_{c3}	0.7902	N m	2.7986
f_{c4}	1.0394	N m	2.1046

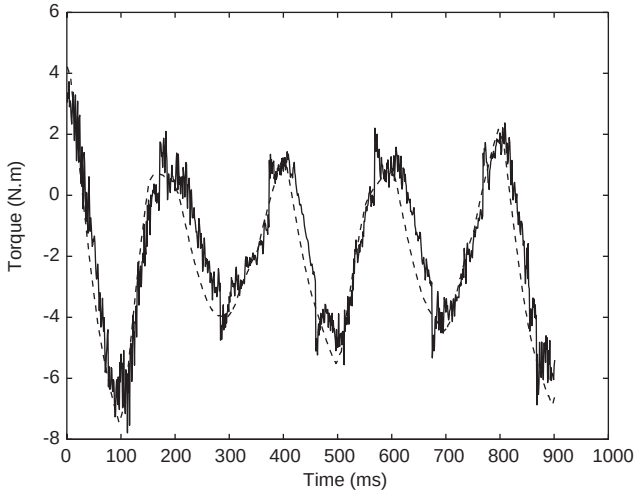

Fig. 5. Estimated and measured torques for motor 1.

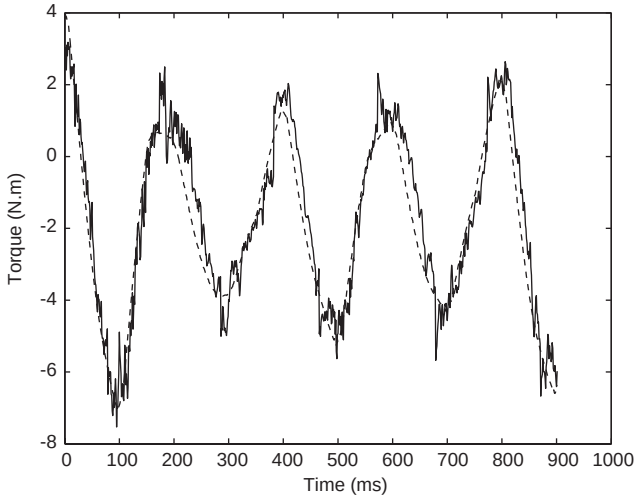

Fig. 6. Estimated and measured torques for motor 2.

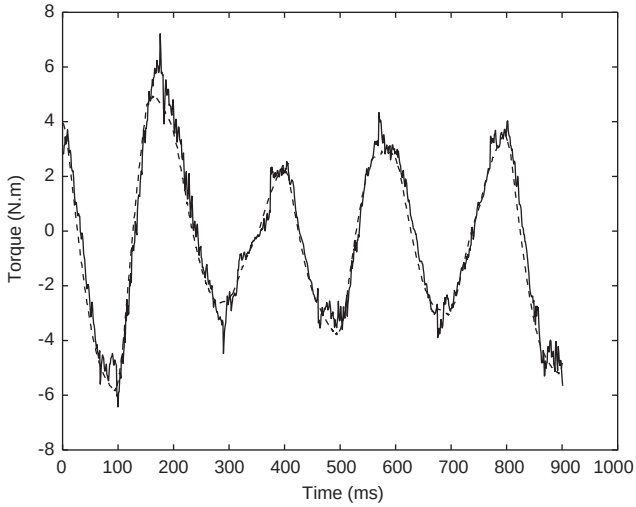

Fig. 7. Estimated and measured torques for motor 3.

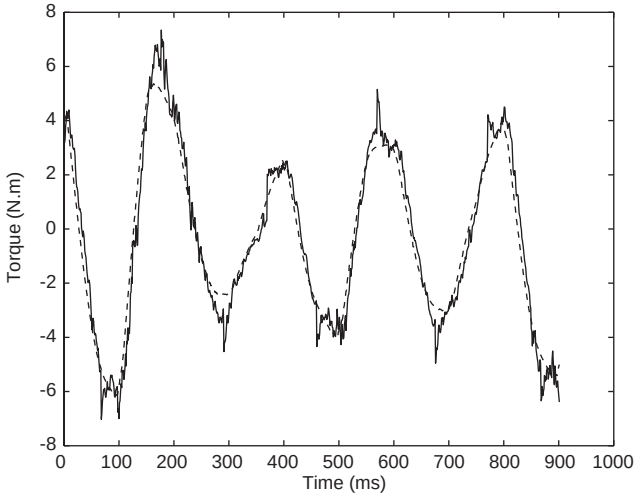

Fig. 8. Estimated and measured torques for motor 4.

identification. Estimated torques and measurements are very close.

6. Conclusion

In this paper, we present the comprehensive identification of the complete physical model of a parallel robot. In a first step, the kinematic parameters are identified using vision as a sensor for the position and orientation in space of the end-effector. Thus, static accuracy is lowered from some 1 cm down to 1 mm. Then, using the identified kinematic parameters, dynamic parameters are identified yielding an estimation of the input control torques within $\pm 10\%$ of the measured ones.

In the next future, we plan to extend the vision measurements to higher frequencies (≈ 1 kHz), so that we can use them in the dynamic identification. This would then open the way to a method which would simultaneously identify the kinematic and the dynamic parameters, rather than in two steps as in the present method. However, such a simultaneous method will probably not be efficient if the associated tough problems of identifiability and excitation cannot be solved.

References

Andreff, N., Espiau, B., & Horaud, R. (2002). Visual servoing from lines. *International Journal of Robotics Research*, *21*(8), 679–700.

Andreff, N., Horaud, R., & Espiau, B. (2001). Robot hand-eye calibration using structure-from-motion. *International Journal of Robotics Research*, *20*(3), 228–248.

Besnard, S., & Khalil, W. (2001). Identifiable parameters for parallel robots kinematic calibration. In *International conference on robotics and automation* (pp. 2859–2866), Seoul, Korea.

Company, O., & Pierrot, F. (1999). A new 3T-1R parallel robot. In *Proceedings of ICAR'99*, Tokyo, Japan, October 1999.

Daney, D. (1999). Self calibration of Gough platform using leg mobility constraints. In *World congress on the theory of machine and mechanisms* (pp. 104–109), Oulu, Finland.

Daney, D. (2002). Optimal measurement configurations for Gough platform calibration. In *International conference on robotics and automation* (pp. 147–152), Washington DC.

Gautier, M. (1991). Numerical calculation of the base inertial parameters. *Journal of Robotics Systems*, *8*(4), 485–506.

Gautier, M. (2000). Optimal motion planning for robot's inertial parameters identification. In *Proceedings of the 31st CDC*, Tucson, USA.

Gautier, M., & Khalil, W. (1990). Direct calculation of the minimum inertial parameters of serial robots. *Transactions on Robotics and Automation*, *6*(3), 368–373.

Gautier, M., & Khalil, W. (1992). Exciting trajectories for the identification of base inertial parameters of robots. *International Journal of Robotics Research*, *11*(4), 362–375.

Gautier, M., & Poignet, Ph. (2001). Extended Kalman filtering and weighted least squares dynamic identification of robot. *Control Engineering Practice*, *9*(12), 1361–1372.

Geng, Z. J., & Haynes, L. S. (1994). A "3-2-1" kinematic configuration of a Stewart platform and its application to six degrees of freedom pose measurements. *Robotics and Computer-Integrated Manufacturing*, *11*(1), 23–34.

Jeong, J. W., Kim, S. H., & Kwak, Y. K. (1999). Kinematics and workspace analysis of a parallel wire mechanism for measuring a robot pose. *Mechanism and Machine Theory*, *34*, 825–841.

Khalil, W., & Besnard, S., 1999. Self calibration of Stewart–Gough parallel robots without extra sensors. Transactions on Robotics and Automation, 1758–1763.

Khalil, W., & Dombre, E. (2002). *Modeling identification and control of robots*. London: Taylor and Francis.

Khalil, W., & Murareci, D. (1997) Autonomous calibration of parallel robots. In *Fifth IFAC symposium on robot control* (pp. 425–428), Nantes, France.

Koseki, Y., Arai, T., Sugimoto, Takatuji, T., & Goto, M. (1998). Design and accuracy evaluation of high-speed and high-precision parallel mechanism. In *International conference on robotics and automation* (pp. 1340–1345), Leuven, Belgium.

Lavest, J. M., Viala, M., & Dhome, M. (1998). Do we really need an accurate calibration pattern to achieve a reliable camera calibration. In *European conference on computer vision* (*ECCV'98*) (pp. 158–174), Freiburg, Germany.

Merlet, J.-P. (2000). *Parallel robots*. Dordrecht: Kluwer Academic Publishers.

Masory, O., Wang, J., & Zhuang, H. (1993). On the accuracy of a Stewart platform—part II kinematic calibration and compensation. In *International conference on robotics and automation* (pp. 725–731), Atlanta.

Nahvi, A., & Hollerbach, J. M. (1996). The noise amplification index for optimal pose selection in robot calibration. In *International conference on robotics and automation* (pp. 647–654), Minneapolis, Minnesota.

Olsen, M. M., & Petersen, H. G. (2001). A new method for estimating parameters of a dynamic robot model. *Transactions on Robotics and Automation*, *17*(1), 95–100.

Pierrot, F., Marquet, F., Company, O., & Gil, T. (2001). H4 parallel robot: Modeling, design and preliminary experiments. In *International conference on robotics and automation* (pp. 3256–3261), Seoul, Korea.

Renaud, P. (2003). *Apport de la vision pour l'identification géométrique de mécanismes parallèles*. Ph.D. Thesis, University Blaise Pascal, Clermont-Ferrand.

Renaud, P., Andreff, N., Gogu, G., & Dhome, M. (2003). Optimal pose selection for vision-based kinematic calibration of parallel mechanisms. In *International conference on intelligent robots and*

systems (*IROS*) (pp. 2223–2228), Las Vegas, Nevada, October 2003.

Schroer, K. (1993). In *Robot calibration*, R. Bernhardt and S.L. Albright (eds.), Theory of kinematic modelling and numerical procedures for robot calibration (pp. 157–196), London: Chapman & Hall.

Swevers, J., Ganseman, C., Tükel, B. D., De Schutter, J., & Van Brussel, H. (1997). Optimal robot excitation and identification. *Transactions on Robotics and Automation*, *13*(5), 730–740.

Vincze, M., Prenninger, J. P., & Gander, H. (1994). A laser tracking system to measure position and orientation of robot end-effectors under motion. *International Journal of Robotics Research*, *13*(4), 305–314.

Visher, P. (1996). *Improve the accuracy of parallel robot*. Ph.D. Thesis, EPFL, Lausanne.

Wampler, C., & Arai, T. (1992). Calibration of robots having kinematic closed loops using non-linear least-squares estimation. In *IFTOMM world congress in mechanism and machine science* (pp. 153–158), Nagoya, Japan, September 1992.

Wampler, C. W., Hollerbach, J. M., & Arai, T. (1995). An implicit loop method for kinematic calibration and its application to closed-chain mechanisms. *Transactions on Robotics and Automation*, *11*(5), 710–724.

Wang, J., & Masory, O. (1993). On the accuracy of a Stewart platform—Part I: The effect of manufacturing tolerances. In *International conference on robotics and automation* (pp. 114–120), Atlanta.

Zhuang, H. (1997). Self-calibration of parallel mechanisms with a case study on Stewart platforms. *Transactions on Robotics and Automation*, *13*(3), 387–397.

Zhuang, H., Masory, O., & Yan, J. (1995). Kinematic calibration of a Stewart platform using pose measurements obtained by a single theodolite. In *International conference on intelligent robots and systems* (pp. 329–334), Pittsburgh.

Zhuang, H., & Roth, Z. S. (1996). *Camera-aided robot calibration*. Boca Raton, FL: CRC Press.

Zhuang, H., Yan, J., & Masory, O. (1998). Calibration of Stewart platforms and other parallel manipulators by minimizing inverse kinematic residuals. *Journal of Robotic Systems*, *15*(7), 395–405.

Zou, H., & Notash, L. (2001). Discussions on the camera-aided calibration of parallel manipulators. In *Proceedings of the 2001 CCToMM symposium on mechanisms, machines, and mechatronic*, Saint-Hubert.